Received: 24 February 2019 | Revised: 20 June 2019 | Accepted: 29 July 2019

DOI: 10.1111/jace.16764



Journal of the American Ceramic Society

REGULAR ARTICLE

# PVA- and PEG-assisted sol-gel synthesis of aluminosilicate precursors for N-A-S-H geopolymer cements

**Juan Pablo Gevaudan**[1] | **Jaqueline D. Wallat**[1] | **Bimala Lama**[2] | **Wil V. Srubar III**[1,3]

[1]Department of Civil, Environmental, and Architectural Engineering, University of Colorado Boulder, Boulder, Colorado

[2]Department of Chemistry, University of Colorado Boulder, Boulder, Colorado

[3]Materials Science and Engineering Program, University of Colorado Boulder, Boulder, Colorado

**Correspondence**
Wil V. Srubar III, 1111 Engineering Drive, ECOT 441 UCB 428, Boulder, CO 80309.
Email: wsrubar@colorado.edu

**Funding information**
National Science Foundation, Grant/Award Number: CBET-1604457 and CMMI-1727788

**Abstract**

This study investigates critical factors affecting polymer-assisted sol-gel synthesis of synthetic aluminosilicate powders that can be alkali-activated to produce a sodium-stabilized aluminosilicate hydrate (N-A-S-H) geopolymer cement. More specifically, a $2^2$ factorial experiment was conducted to elucidate the influence of polymer architecture (ie, poly(ethylene glycol) (PEG) vs poly(vinyl alcohol) (PVA)), polymer content (ie, low vs high ion-to-polymer-oxide (I/O) atomic ratio), and sol-gel aging pH conditions (ie, low vs high) on the atomic structure of resultant synthetic aluminosilicate powders and geopolymer cements. Molecular structure was investigated using solid-state (single-pulse and $^1$H cross-polarization) $^{29}$Si and $^{27}$Al nuclear magnetic resonance (NMR) and Fourier-transform infrared (FTIR) spectroscopy. The mineralogy of geopolymer cements was assessed with X-ray diffraction and compared to alkali-activated metakaolin-based cements of equivalent stoichiometry. Results demonstrate that polymer architecture (PEG vs PVA) is a key factor in producing (a) undesirable phase segregation (ie, $\gamma$-alumina) and (b) incomplete dehydroxylation (ie, vicinal silanol) in synthetic aluminosilicate powders. More specifically, PEG-derived aluminosilicate powders yield partial dissolution and produce geopolymer cements with variable silicate incorporation. Contrastingly, PVA-derived aluminosilicate powders produce geopolymer cements with identical mineralogy to that of metakaolin-based geopolymer cements and exhibit both Brønsted-acid sites near the aluminum nuclei and geminal silanol groups. Sol-gel aging pH conditions reveal the ability to influence the hydroxyl group content, which is an important factor affecting the durability of cementitious materials. Lastly, three plausible mechanisms of metal complexation are hypothesized to permit incorporation of solubilized metal ions *via* a polymer-assisted sol-gel process.

**KEYWORDS**

alkali activation, geopolymers, metakaolin, nuclear magnetic resonance, sol-gel synthesis

## 1 | INTRODUCTION

Polymer-assisted sol-gel synthesis—otherwise known as the organic steric entrapment (OSE) method—was first demonstrated in 1992 as a viable method to produce metal-oxide ceramics. Earlier, in 1931, conventional (ie, nonpolymer-assisted) sol-gel synthesis methods were used to produce ceramics using alkoxysilanes.[1,2] The primary aim of sol-gel synthesis is to produce solid ceramics from a solution of liquid metal precursors *via* hydrolysis and subsequent polycondensation into a gel.[3] By forming gels in a solution state, sol-gel synthesis methods ensure atomic-level mixing, thereby circumventing challenges

  

associated with solid-state chemistry (eg, inhomogeneity, phase separation, low-yield reactions).[3,4] As a departure from conventional sol-gel synthesis, polymer-assisted sol-gel synthesis was first reported in a study that used poly(ethylene glycol) (PEG) to synthesize nanocrystalline Perovskite materials.[5,6] Soon thereafter, poly(vinyl alcohol) (PVA) was used to produce fine ferrite powders and mixed-metal-oxide materials.[7–10] In 1999, polymer-assisted sol-gel synthesis was renamed the OSE method, due to the speculation that weak hydrogen bonding between the polymer and metal oxides was primarily responsible for sterically entrapping and structuring solvated cations in solution.[11,12]

OSE has since been used to synthesize metal-oxide precursors to traditional ordinary portland cement (OPC) cementitious binders, as well as alternative cementitious binders such as calcium- and sodium-stabilized aluminosilicate hydrates (ie, C-N-A-S-H and N-A-S-H).[13–15] Examples of synthesized OPC phases include calcium aluminate, dicalcium silicate, tricalcium silicate, tricalcium aluminate, and tetracalcium aluminate iron oxide.[11,16] These synthesized cementitious components were found to be pure, nano-, or sub-micron sized and highly reactive. Furthermore, recent renewed interest in this synthesis method has arisen due to the possibility of producing alternative cementitious binders (ie, calcium aluminosilicate hydrates and sodium aluminosilicate binders).[13,14,17,18] The production of alternative cementitious binders through OSE presents a unique opportunity to understand the influence of atomic structure on material properties *via* precise stoichiometric control of the alternative cement chemistry.[19]

Despite advances in polymer-assisted sol-gel synthesis, the effect of processing conditions to produce aluminosilicate precursors that yield structural variants of N-A-S-H cementitious binders is not well understood. Such N-A-S-H cementitious binders, or geopolymer cements, have gained popularity for their controllable chemistry and potential for increased durability, improved fire resistance, and reduced environmental impacts compared to OPC in some applications.[20–22] Traditionally, geopolymer materials are composed of N-A-S-H binders, which have a standard composition of $SiO_2/Al_2O_3 = 3.3$, $Na_2O/Al_2O_3 = 1.1$, and $H_2O:Na_2O = 11$[23] with modern N-A-S-H binders having $SiO_2/Al_2O_3$ between 0.5 and 2.0 given the choice of low-calcium precursor. Multiple studies have been pivotal to understand the atomic structure and properties of N-A-S-H binders as well as dictating the foundation for synthesizing such binders *via* polymer-assisted sol-gel methods using PVA as the polymer cross-linking agent.[13,18,19,24–26] However, little scientific understanding on process-structure effects of different N-A-S-H precursor synthesis conditions currently exists.

The aim of this study was to elucidate process-structure relationships of synthetic aluminosilicate powders produced *via* polymer-assisted sol-gel synthesis, as well as process-structure relationships of resultant sodium-stabilized aluminum-silicate-hydrate (N-A-S-H) geopolymer cements. The influence of synthesis processing factors (ie, polymer architecture, polymer content, and sol-gel aging pH) were explored using a $2^2$ factorial design to reveal changes in atomic structure and variations in mineralogy in both synthetic aluminosilicate powders and resultant geopolymer cements. Lastly, the mineralogy of geopolymer cements is compared to that of alkali-activated metakaolin-based cements. Figure 1 illustrates the scope of work and nomenclature used in this study.

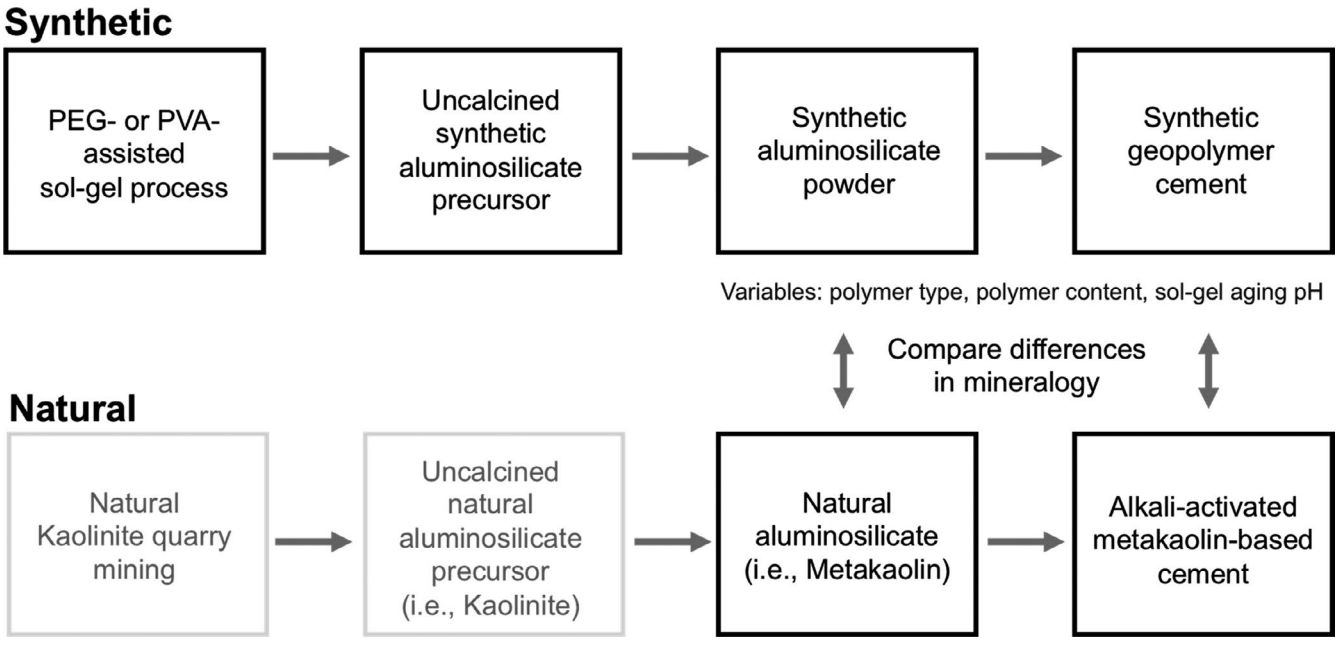


**FIGURE 1** Scope of work and nomenclature used for this study

## 2 | EXPERIMENTAL PROGRAM

### 2.1 | Materials

Polyvinyl alcohol and PEG polymers of molecular weight 31-50 kDa ($M_w$) and 35 kDa ($M_n$), respectively, were obtained from MilliporeSigma. Aluminum nitrate nonahydrate (99+%, analysis grade, Acros Organics), a 40% by weight colloidal silica suspension (LUDOX TM-40, Millipore), sodium hydroxide (NaOH) (10 mol/L, BioUltra grade, MilliporeSigma), and NaOH (reagent grade) were also acquired from MilliporeSigma. Metakaolin (Si:Al = 1.0) was supplied by BASF Chemical Corporation (MetaMax).

### 2.2 | Experimental methods

#### 2.2.1 | $2^2$ factorial design

The influence of both polymer architecture and sol-gel aging pH was investigated using a $2^2$ factorial design of experiments. Additionally, the influence of polymer content was explored in combination with the aforementioned factors. In terms of polymer architecture, both PEG and PVA of similar molecular weights were used to elucidate the role of polymer architecture. Sol-gel aging at two different pH conditions (low pH ~ 1.0, high pH ~ 10) explored pH-dependent metal-polymer interactions. Polymer content was explored by varying the ion-to-polymer-oxide atomic ratios (I/O) in two levels (see Supplementary Information for calculation of I/O). The "ion" content refers to aluminum metal ions, while the oxide solely refers to the polymer oxide content. The aluminum content of aluminum nitrate nonahydrate salts was determined to be 9.28 wt% via ICP-OES and used to calculate accurate I/O ratios. As seen in Table 1, PVA-derived precursors had I/O ratios of 4.0 (low) and 5.2 (high), while PEG-derived precursors had I/O ratios of 3.7 (low) and 4.4 (high). While similar ratios have been described as metal-to-hydroxide (M/OH) atomic ratios, in the present study, PVA chain hydroxyls are compared to PEG chain ethers and, as a result, a redefinition of this atomic ratio was used to account for the differences in polymer architecture as an I/O ratio, where oxide (O) accounts for ethers or hydroxyls.

#### 2.2.2 | Polymer-assisted sol-gel synthesis and characterization of aluminosilicate precursors

Aluminosilicate precursors were synthesized following the polymer-assisted sol-gel procedure developed by Ref. [18]. As explained earlier, the herein methodology mainly differs from Ref. [18] by exploring the effect of polymer content (I/O ratio) as well as sol-gel aging pH condition. PEG and PVA polymeric solutions of 5% (by weight) were produced by incrementally adding the polymer to deionized water over heat (~90°C). Once the polymer was completely dissolved, verified by visual inspection, the solutions were left to age for 1 hour at a temperature of 60°C to 70°C. Synthesis pH during sol-gel aging was controlled at two conditions either low pH (~1.0) or high pH (~10.0) via order of reactant addition. For example, high-pH samples were synthesized by first adding the colloidal silica suspension reactant and allowing the polymer to interact with the reactant for 1 hour (sol-gel aging time) at a pH ~10 (sol-gel aging condition). After 1 hour of sol-polymer interactions at high pH, a 40% (by weight) solution of aluminum nitrate nonahydrate solution was added, which decreased the pH to ~1.0. For low-pH samples, addition of the aluminum nitrate nonahydrate solution was performed first and left to interact with the polymer for 1 hour before addition of the colloidal silica solution. The sol-gel synthesis conditions remained at a pH of ~1.0. After the sol-gel aging process, all solutions were dried via continuous stirring over heat (70°C to 80°C), during which a viscous and porous xerogel was formed. Samples of the xerogels (ie, uncalcined synthetic aluminosilicate powders) were collected for subsequent characterization.

**TABLE 1** Processing parameters and corresponding surface area ($m^2/g$) of synthesized aluminosilicate powders with $2SiO_2 \cdot Al_2O_3$ stoichiometry

| Sample | Polymer molecular weight (kDa) | Aging condition (pH) | Polymer content (I/O ratio) | BET surface area ($m^2/g$) |
|---|---|---|---|---|
| PVA-L | 31-50 | ~1.0 (Low) | 4.0 (Low) | 127.3 ± 0.2 |
| | 31-50 | ~1.0 (Low) | 5.2 (High) | 121.4 ± 0.3 |
| PVA-H | 31-50 | ~10.0 (High) | 4.0 (Low) | 107.9 ± 0.9 |
| | 31-50 | ~10.0 (High) | 5.2 (High) | 130.8 ± 0.3 |
| PEG-L | 35 | ~1.0 (Low) | 3.7 (Low) | 129.6 ± 0.6 |
| | 35 | ~1.0 (Low) | 4.4 (High) | 132.6 ± 0.7 |
| PEG-H | 35 | ~10.0 (High) | 3.7 (Low) | 141.9 ± 0.9 |
| | 35 | ~10.0 (High) | 4.4 (High) | 121.7 ± 0.5 |

### 2.2.3 | Surface area characterization of aluminosilicate precursors

Further following the procedure developed by Ref. [18], both PVA and PEG xerogels were calcined at 550°C and 900°C, respectively, with a hold time of 1 hour (ramp rate of 3°C/min). The resultant white material was ground to form a powder and sieved through a No. 100 sieve. Samples of the synthetic aluminosilicate powders were saved for subsequent characterization. The Brunauer-Emmett-Teller (BET) nitrogen adsorption method was used to measure the surface area of the calcined powders. Samples were massed and degassed under vacuum in an inert nitrogen atmosphere at 100°C for at least 8 hours. After conducting a blank acquisition, samples were placed into the instrument and nitrogen gas was deposited atop the powder surface by varying the $N_2$ pressure. For the measurement, 11 data points were collected with relative pressure ($P/P_o$) ranging from 0.05 to 0.30 with a 5 second equilibration time. From the data, a BET plot was generated using a linear regression with a correlation coefficient of 0.99 for all data generated. The surface area of the resulting powders is reported in Table 1. The surface area measurements herein are similar to those reported for in comparable literature.[18,27]

### 2.2.4 | Geopolymerization of synthetic and natural precursors

Aluminosilicate powders were alkali-activated via addition of NaOH (10 mol/L, BioUltra grade, MilliporeSigma) at a liquid-to-solid weight ratio of 0.75 to form synthetic geopolymers cements, as similarly reported in Ref. [19,28]. Geopolymers were produced by manual mixing for 1 minute until a homogenous paste was obtained. Additionally, natural metakaolin-based geopolymer cements were utilized for mineralogical comparison. The mixing procedure consisted of an initial 1 minute of manual mixing, followed by 1 minute of mechanical mixing using a Waring PDM112 mixer and 1 minute of additional manual mixing to ensure that all of the dry components were mixed homogenously.

The natural metakaolin-based geopolymer cements were designed to exhibit equal chemical parameters as the synthetic geopolymer cements. More specifically, NaOH (reagent grade) was dissolved in deionized water to create activating solutions and yield Si:Al and Na:Al ratios of metakaolin-based geopolymer cements of 1.0 and 1.1, respectively. Both natural and synthetic geopolymer cements were cast in cylindrical molds (diameter: 1.26 cm, height: 3 cm) and cured at 35°C ± 5°C and 100% relative humidity for 48 ± 4 hours in a Quincy forced-air laboratory oven. Subsequently, samples were dried at 30°C overnight (>12 hours) as previously investigated by our research group on calcium-free AAC formulations by Ref. [29].

### 2.2.5 | $^{29}$Si and $^{27}$Al solid-state magic angle spinning nuclear magnetic resonance (MAS NMR)

Solid-state $^{29}$Si and $^{27}$Al MAS NMR spectra were acquired using a Varian INOVA 400 MHz NMR spectrometer (magnetic field 9.39 T; operating frequency of 79.50 MHz for $^{29}$Si and 104.27 MHz for $^{27}$Al). Samples were packed into 4 mm zirconia rotors sealed at either end with Teflon end plugs, and all spectra were collected with MAS speed of 10 kHz using a broadband probe equipped with a 4 mm MAS spinning module designed and manufactured by Revolution NMR, LLC (Fort Collins, CO). $^{29}$Si chemical shifts were determined using the NMR signal from DSS (2,2-dimethyl-2-silapentanesulfonate) referenced at 1.46 ppm. The spectra were acquired through a Bloch-decay experiment with 1600 scans using a pulse recycle delay of 5 seconds, a pulse width of 4.5 μs, and an acquisition time of ~20 ms. These experimental parameters are sufficient for the qualitative analysis of the data, as presented herein. Cross-polarization (CP) MAS data were also collected using $^{1}$H and $^{29}$Si 90° pulse widths of 3.8 and 4.5 μs, respectively, with recycle delay of 2 seconds, CP spin-lock time of 3 ms, and 1600 scans. The $^{27}$Al chemical shifts were referenced to aluminum nitrate (0.0 ppm) and the Bloch-decay experiment was acquired using a pulse recycle delay of 5 seconds, a pulse width of 4.5 μs, an acquisition time of ~ 20 ms, and 256 scans. For cross-polarization ($^{1}$H–$^{27}$Al) MAS experiments, $^{1}$H and $^{13}$C 90° pulse widths of 3.8 and 4.5 μs, respectively, were used with a recycle delay of 2 seconds, CP spin-lock time of 2 ms, and 256 scans. Peak identification and data processing were performed using MestReNova software.

### 2.2.6 | Inductively coupled plasma optical emission spectrometry (ICP-OES)

Chemical characterization was determined with an ICP-OES (ARL 3410+) using an adapted protocol from a widely accepted technique developed by Farrell et al.[30] Five mL of a 7:3 mixture of hydrochloric acid and hydrofluoric acid were combined with 2 mL of nitric acid and placed in digestion tubes that were maintained at 95°C in a digestion block (HotBlock by Environmental Express) for approximately 2 hours. Samples were then cooled and brought to 50 mL with a 1.5% boric acid solution (by mass). The samples were then reheated to 95°C for 15 minutes and cooled for analysis. The samples were diluted 10× with deionized water and analyzed with an ICP-OES, as described above. An analytical blank, along with three standards that were made by accurately diluting certified standards, was used for calibration. Finally, a basaltic internal standard (Valmont Dike, Colorado USA) of known chemical composition was digested and analyzed to ensure accuracy of the results.

### 2.2.7 | Fourier-transform infrared spectroscopy (FTIR)

Samples for analysis were ground in a slurry of ethanol using a McCrone micronizing mill with yttrium-stabilized zirconium (American Elements) grinding beads for 5 minutes to ensure particle sizes <5 μm. Collected slurries were dried overnight at 60°C. Next, 0.02 ± 0.005 g of each sample were mixed with 2.00 ± 0.050 g of potassium bromide (KBr) powder (dried at 70°C overnight). Then, the powder mixtures were homogenized in a Spex Grinder mill and pressed into KBr disk pellets for analysis in a Thermo Scientific Nicolet iS10 FTIR Spectrometer. As a result, KBr disks with sample concentrations of 1% (by weight) were produced. Disks were analyzed against a blank background to remove the absorption spectra from the chamber purged with nitrogen.

### 2.2.8 | X-ray diffraction (XRD)

To determine the mineralogy of (a) calcined precursors and (b) both synthetic and natural alkali-activated geopolymer binders, samples were first crushed into a powder with a mortar and pestle. The calcined precursor and synthetic geopolymer binder powders were well packed in XRD sample holders. Metakaolin-based geopolymer binders were prepared for mineral analysis using a modified method based on Ref. [31]. The former method was modified to employ corundum as an internal standard instead of zincite. All samples were analyzed in a Siemens D500 X-ray diffractometer to acquire X-ray diffraction patterns for all samples. Samples were analyzed from 5° to 65° 2$\theta$ using Cu$K\alpha$ X-ray radiation, with a step size of 0.02° and a dwell time of 2 seconds per step. Mineralogy was identified using Jade software (MDI, Version 9) and the International Centre for Diffraction Data (ICDD) 2003 database.

## 3 | EXPERIMENTAL RESULTS AND ANALYSIS

### 3.1 | Stoichiometry of geopolymer cements

Synthesized geopolymer cements in the herein study have uniform chemical formulations of $Na_{1.22}Si_{1.02}Al{\cdot}xH_2O$, see Figure 2. As a result, the stoichiometry of geopolymer cements yields Si:Al and Na:Al atomic ratios of 1.02 ± 0.07 and 1.22 ± 0.07, respectively, regardless of polymer cross-linking agents (PEG and PVA), synthesis pH conditions (low and high) or I/O ratios (low and high). This chemical composition is similar to the theoretical design composition outlined in Section 2.2.4 and bears important differences from "traditional" geopolymer materials, which are reported to have a standard composition of Si:Al = 1.65 and Na:Al = 1.[23] As

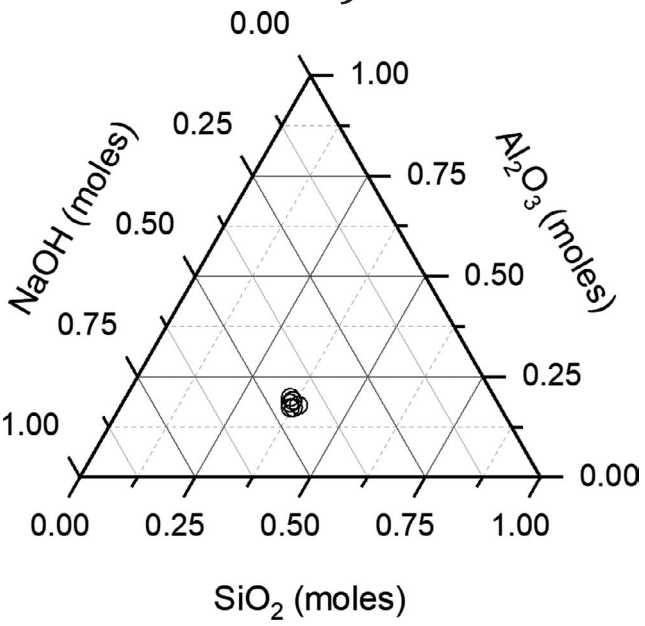


**FIGURE 2** Chemical composition of all geopolymer cements synthesized from synthetic aluminosilicate precursors. Average values for Si:Al and Na:Al atomic ratios are 1.02 ± 0.07 and 1.22 ± 0.07, respectively

a result, important morphological differences exist due to their "non-traditional" cement chemistry, as expected from literature.[14,27,32] For example, the presence of mineral phases, such as zeolites, is expected at low silicon and high sodium contents when these samples are subjected to hydrothermal curing conditions.[33]

### 3.2 | Mineralogy of aluminosilicate powders and geopolymer cements

Regardless of synthesis pH and I/O ratio, mineralogical differences were only observed in samples produced with different polymers (Figure 3). PVA-derived synthetic aluminosilicate powders demonstrate an amorphous curve at 23° 2$\theta$ angles and, after alkali-activation, the geopolymer cements result in the formation of zeolite A and sodium carbonate. Contrastingly, PEG-derived synthetic aluminosilicate powders demonstrate the formation of alumina phases, in addition to the aforementioned amorphous curve at 23° 2$\theta$ angles. After alkali-activation, PEG-derived geopolymer cements result in the formation of sodium carbonate solely and no alumina phases diffraction patterns are observed. Hence, these results provide evidence of phase segregation, an undesirable product of in homogeneity during reaction (4), as a result of the presence of ethers (ie, C–O) in the PEG polymer cross-linker, which likely do not coordinate $Al^{+3}$ ions as effectively as hydroxyl groups (ie, O–H) of PVA polymers. Only synthetic aluminosilicate powders derived from PEG polymer cross-linkers

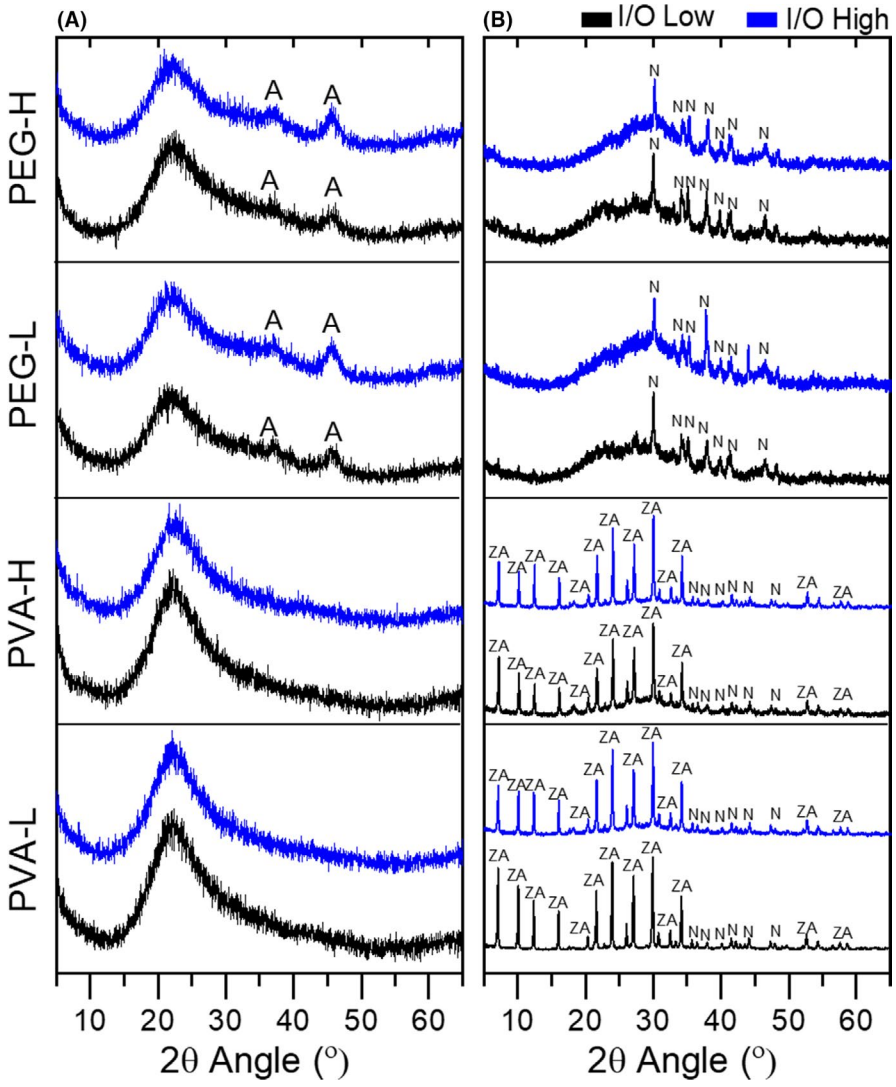


**FIGURE 3** Mineralogy for (A) synthetic aluminosilicate powders and (B) alkali-activated geopolymer cements. Symbols represent mineral formations as follows—A: $\gamma$-alumina ($Al_2O_3$, PDF#01-074-2206), ZA: Zeolite A ($Al_2O_3SiO_2$, PDF# 00-038-0323), N: Sodium Carbonate ($Na_2CO_3$, PDF#01-072-0628)[38,39] [Color figure can be viewed at wileyonlinelibrary.com]

result in the formation of alumina phases, as indicated by XRD (Figure 3). Given the high-temperature calcination (ie, 900°C) for PEG-derived synthetic aluminosilicate powders, the alumina phase in Figure 3 likely is that of $\gamma$-alumina. This alumina mineral forms due to dehydration between 500°C and ~900°C,[34] as well as temperatures of up to 1200°C,[35] and has a similar diffraction pattern as $\eta$-alumina.[36,37]

### 3.3 | FTIR of synthetic precursors, aluminosilicate powders, and geopolymer cements

To probe the molecular structure of all synthesized materials, FTIR was undertaken. For this study, FTIR was collected for each of the samples throughout the reaction (Figure 4) and compared to reagent materials (Figures S1-S10). In agreement with XRD diffractograms (Figure 3), carbonation is evident in the FTIR spectra by a large vibrational peak at 1470 $cm^{-1}$ corresponding to O–C–O stretching of carbonate, which appears mainly for PEG-derived geopolymer cements as indicated by Figure 4 and Table 2.

For PVA-derived uncalcined synthetic aluminosilicate precursors, regardless of pH or I/O, vibrational energy bands are observed with relatively the same peak location and peak intensity (Figure 4). Key vibrational bands for PVA-derived products throughout the reaction are listed in Table 2. When compared to the uncalcined synthetic aluminosilicate precursor, the synthetic aluminosilicate powders show (a) a decrease in O–H, C–O, and C–H bond vibrational stretching (3500-3000 $cm^{-1}$, 2925 $cm^{-1}$, 2850 $cm^{-1}$, 1730 $cm^{-1}$, and 1645 $cm^{-1}$); (b) minor changes to the presence of N–O or O–C–O bond asymmetric stretching (1475 and 1380 $cm^{-1}$); and (c) the presence of Al–O and Si–O–Si bonds (1116, 904, 932, 722-540, and 480 $cm^{-1}$). Upon alkali-activation, there are a number of key differences in the vibrational energy bands of the resulting materials, (a) the emergence of O–C–O and O–H vibrations due to carbonation and hydration of the cementitious material (1651, 1550, 1475, and 1380 $cm^{-1}$); (b) external linkage of $SiO_4$

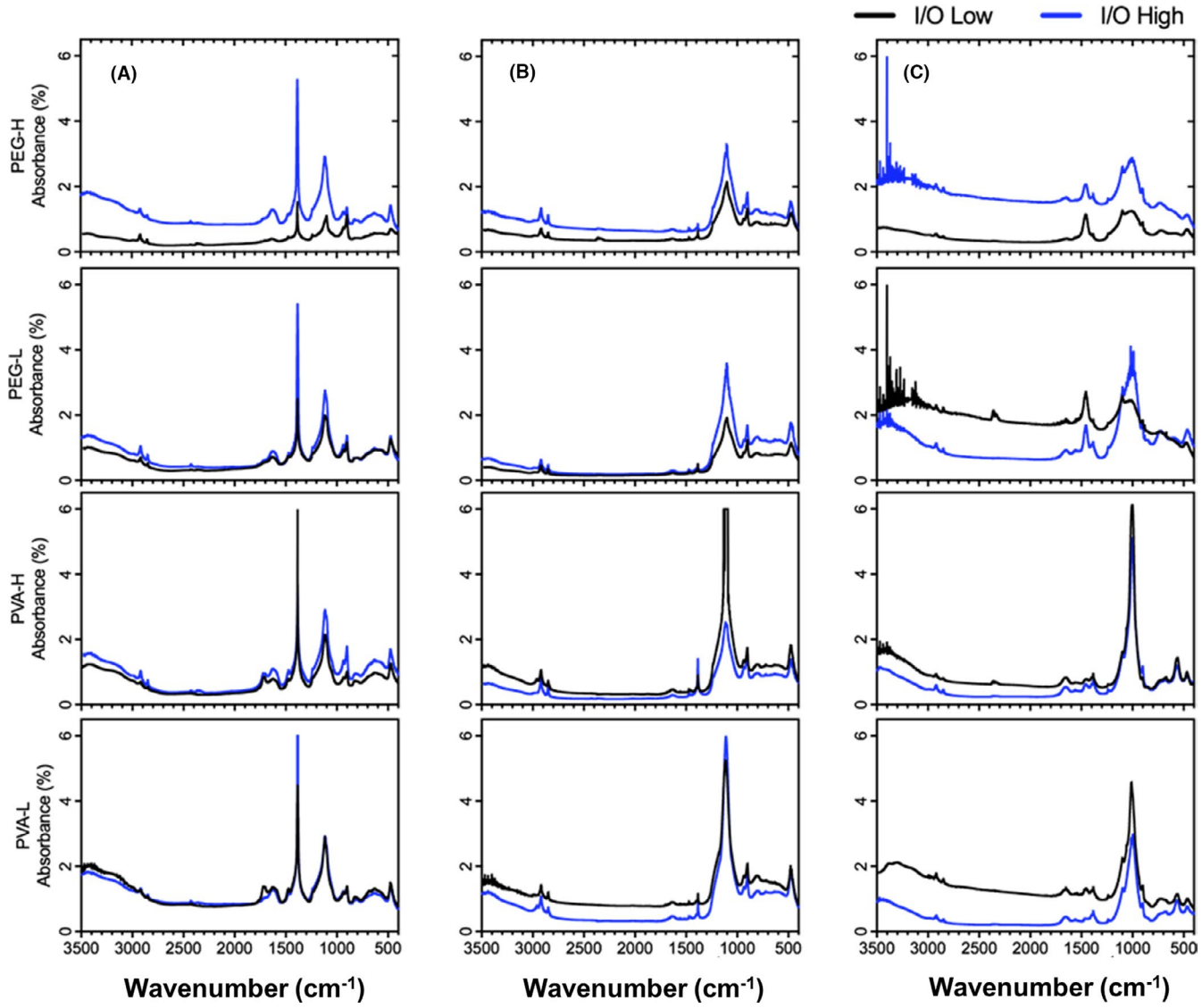


**FIGURE 4** Fourier-Transform Infrared Spectroscopy of (A) uncalcined synthetic aluminosilicate precursors, (B) synthetic aluminosilicate powders, and (C) geopolymer cements [Color figure can be viewed at wileyonlinelibrary.com]

and $AlO_4$ tetrahedral (560 $cm^{-1}$); and moreover, (c) aluminosilicate network formation (Si–O–Al) signified by a shift in frequency of peak toward 1000 $cm^{-1}$, which have traditionally been attributed to geopolymer formation[51,52] or zeolite formation from aluminosilicate precursors[40,53] (Table 2). In addition, absorption shoulders at 1116 and 908 $cm^{-1}$ are also identified in geopolymer cements, which indicate asymmetric Si–O stretching and were also observed in synthetic aluminosilicate powders. Such geopolymer network formation as well as external linkage vibration of $Si–O_4$ or $Al–O_4$, typical for zeolites,[41] are also verified by XRD results, shown in Figure 3.

The analysis of the FTIR from PEG-derived systems indicates that for a given processing condition, the material has similar vibrational energy, regardless of pH and I/O. However, key differences in the extent of geopolymer network formation (Si–O–Al) exist, when compared to PVA-derived products. In the uncalcined state, vibrational energy bands for all samples are observed at relatively the same peak location and peak intensity (Figure 4). Key vibrational bands for PEG-derived products throughout the reaction are listed in Table 3. Upon calcination at 900°C, the resulting vibrational energies of the synthetic aluminosilicate powders show (a) a decrease in O–H, C–O, and C–H bond vibrational stretching (3500-3000, 2925, 2850, 2885, 1630, and 1380 $cm^{-1}$); (b) changes in Si–O–Si asymmetric bond stretching peak (1115 and 1240 $cm^{-1}$); and moreover, (c) the presence of Al–O and Si–O–Si bonds (900, 940, 840-515, and 480 $cm^{-1}$). Upon alkali-activation, there are a number of key differences in vibrational energy band location and intensity, in particular (a) the emergence of O–C–O and O–H vibrations due to carbonation and hydration of the cementitious material (1450 and 1380 $cm^{-1}$); (b) partial reactivity as observed by remaining

**TABLE 2** Analysis of infrared vibrational bands in PVA-derived products, (br) broad, (s) sharp, weak (w), and (sh) shoulder

| (a) Uncalcined precursor ($cm^{-1}$) | (b) Calcined precursor ($cm^{-1}$) | (c) Geopolymer cement ($cm^{-1}$) | Assignment | References |
|---|---|---|---|---|
| 3500-3000 (br) | Decrease intensity compared to (a) | Increase intensity compared to (b) | O–H vibrational stretching | [40,41] |
| 2925 (w)<br>2850 (sh) | Decrease intensity compared to (a) | Decrease intensity compared to (a) (b) | C–H asymmetric and symmetric stretching | [42] |
| 1730 (w)(sh)<br>1650 (w) | No peak at 1730 or 1645, new peak at 1670 | Peak at 1650 same intensity as (b) | C–O stretching and O–H stretching | [43,44] |
| 1450 (sh)<br>1380 (s)(br) | Decrease intensity compared to (a) | Same intensity compared to (b) | N–O stretching or O–C–O asymmetric stretching ($CO_3^{2-}$) | [42,45,46] |
| 1193 (sh)<br>1122 (s)(br) | Same intensity as (a) | Peak shifts to 1000 (s,b) with 1122 (sh) | Si–O–Si or asymmetric Si–O–Si or Al–O–Si | [47,48] |
| 900 (s) | Same intensity as (a) | Becomes sh to peak centered around 1000 | Al–O, Si–O stretching | [49] |
| 810 (w)(br) | Same intensity as (a) | Decrease intensity compared to (b) | Al–O bending mode of $AlO_4$ | [30] |
| 722-540 (w) | Increase intensity compared to (a) | Peak emerges at 560, decrease intensity 722-540 | Various Si–O–Si vibrations, with 560 an external linkage of Si–$O_4$ or Al–$O_4$ | [45,50] |
| 480 (s,br) | Same intensity as (a) | Decrease intensity compared to (b) | Bending (Si–O–Si and O–Si–O) | [50] |

**TABLE 3** Analysis of infrared vibrational bands in PEG-derived products, (br) broad, (s) sharp, weak (w), and (sh) shoulder

| (a) Uncalcined precursor ($cm^{-1}$) | (b) Calcined precursor ($cm^{-1}$) | (c) Geopolymer cement ($cm^{-1}$) | Assignment | References |
|---|---|---|---|---|
| 3500-3000 (br) | Decrease intensity compared to (a) | Increase intensity compared to (b) | O–H vibrational stretching | [44,54] |
| 2925 (w)<br>2885 (sh) | Decrease intensity compared to (a) | Decrease intensity compared to (a) (b) | C–H asymmetric and symmetric stretching | [42] |
| 1720 (w)(sh)<br>1630 (w) | Decrease intensity compared to (a) | Same intensity as (b) | C–O stretching and O–H stretching | [43,44] |
| 1450 (sh)<br>1380 (s)(br) | Decrease intensity compared to (a) | Same intensity as (b) | N–O stretching or O–C–O asymmetric stretching ($CO_3^{2-}$) | [45,46,55,56] |
| 1240 (sh)<br>1115 (s)(br) | Same intensity as (a) | Peak shifts to 1060 (s,b) with 1122 (sh) | Si–O–Si or asymmetric Si–O–Si or Al–O–Si | [47,48] |
| 900 (s)<br>940 (sh) | Same intensity as (a) | Becomes (sh) to peak centered around 1000 | Al–O, Si–O stretching | [49,57] |
| 810 (w)(br) | Same intensity as (a) | Decrease intensity compared to (b) | Al–O bending mode of $AlO_4$ | [30] |
| 722-540 (w) | Increase intensity compared to (a) | Peak emerges at 720, decrease intensity 722-540 | Various Si–O–Si vibrations, with 560 an external linkage of Si–$O_4$ or Al–$O_4$ | [45,50,58] |
| 480 (s,br) | Same intensity as (a) | Decrease intensity compared to (b) | Bending (Si–O–Si and O–Si–O) | [50] |

Si–O–Si vibrations (720 $cm^{-1}$), which is within the broad distribution of weak resonances seen in the uncalcined synthetic aluminosilicate precursors and synthetic aluminosilicate powders from 840-515 $cm^{-1}$; and (c) aluminosilicate network formation (Si–O–Al) signified by a shift toward a new peak centered around 1060 $cm^{-1}$ with shoulders at approximately 1120 and 900 $cm^{-1}$. As noted for PVA products, these two shoulder locations are consistent with two main peaks in the synthetic precursors (both uncalcined and calcined). However, in the herein PEG samples the observed Si–O–Al absorption peaks at 1060 $cm^{-1}$ are broad with larger shoulder regions at 1120 and 950 $cm^{-1}$. Thus indicating a variable and lower extent of Si–O–Al polymerization following alkali-activation.

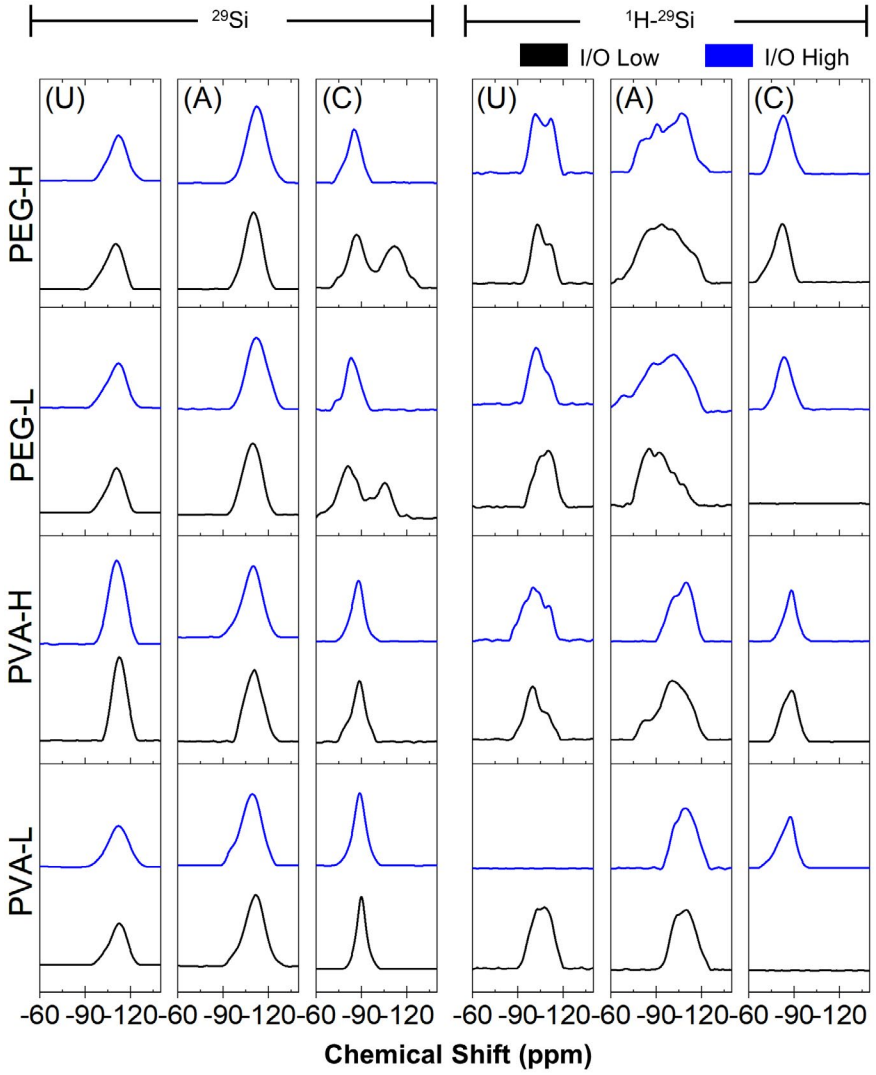


**FIGURE 5** $^{29}$Si MAS NMR and $^{1}$H-$^{29}$Si MAS NMR spectra for uncalcined synthetic aluminosilicate precursors (U), synthetic aluminosilicate powders (A), and geopolymer cements (C) [Color figure can be viewed at wileyonlinelibrary.com]

### 3.4 | $^{29}$Si MAS NMR and $^{1}$H-$^{29}$Si CP MAS NMR of aluminosilicate powders and geopolymer cements

$^{29}$Si CP MAS NMR technique (Bloch Decay) was used to study the silicon atomic structure of synthetic aluminosilicate materials. Figure 5 presents the acquired $^{29}$Si spectra for both uncalcined aluminosilicate precursors and synthetic aluminosilicate powders. The collected spectra reveal the predominance of resonances at chemical shifts of $-112 \pm 0.87$ ppm and $-111 \pm 1.59$ ppm assigned to $Q^4$Si environments in uncalcined and calcined powders, respectively. As a result, calcination revealed no changes to silicon atomic environments.

After alkali-activation, all geopolymer cements indicate a downfield shift in $^{29}$Si signal between $-84$ and $-90$ ppm assigned to $Q^4(4Al)$ atomic environments in the cementitious network. PEG-derived geopolymer cements exhibited an additional resonance at chemical shift of $-107$ ppm corresponding to remaining $Q^4$ from unreacted aluminosilicate powder only when synthesized at low I/O ratios, as seen in Figure 5. Several other key differences exist between both synthesized geopolymer cements. For example, the average chemical shift in PEG-derived geopolymer cements ($-83.67$ ppm) was downfield shifted to a greater extent than that of PVA-derived geopolymer cements ($-89.01$ ppm). Moreover, when compared to all geopolymer cements, PVA-L samples at low I/O ratio demonstrate a narrow linewidth (4.78 ppm) and further upfield shift ($-89.95$ ppm).

$^{1}$H-$^{29}$Si CP MAS NMR experiments were conducted to study the presence of nearby hydrogen atoms to silicon nuclei. In general, PVA- and PEG-derived synthetic aluminosilicate precursors as well as aluminosilicate powders demonstrated a $^{29}$Si resonance of $-105 \pm 5$ ppm in $^{29}$Si CP MAS NMR spectra as expected since cross-polarization techniques allows the resonances only from outer surface of the Al–O–Si network, which are near protons. Because of the inhomogeneous surface structure and nearby hydroxyl group, the peaks are downshifted in comparison to the bulk structure ($-110$ vs $-105$ ppm). This downshift is more

prominent in PEG-derived aluminosilicate powders as they exhibit $^{1}H$-$^{29}Si$ resonances between −100 and −97 ppm confirming the presence of single hydroxyl-containing silica species ($Q^3$). These differences may be explained by the fact that PEG-derived aluminosilicate powders at high polymer contents (low I/O ratio) do not undergo complete dehydroxylation and, thus, remnant single hydroxyls exist ($Q^3$).[55] Furthermore, adjacent water molecules may aid in the deshielding of Si atoms as evidenced by $^{29}Si$ NMR spectra (Figure 5). Similar deshielding has been reported by[43] for Halloysite clays as interlayer water hydrogen bonds to the tetrahedral silicate layers and results in a deshielding of the $^{29}Si$ resonance. Unexpectedly, no $^{1}H$-$^{29}Si$ resonance was observed for PVA-L (high I/O) synthetic aluminosilicate precursors, which indicate the absence of near protons to effectively cross-polarize Si.

### 3.5 | $^{27}Al$ MAS NMR and $^{1}H$-$^{27}Al$ MAS NMR of aluminosilicate powders and geopolymer cements

$^{27}Al$ MAS NMR experiments were conducted to study the changes in aluminum atomic structure of synthetic aluminosilicate materials. All $^{27}Al$ MAS NMR spectra of uncalcined synthetic aluminosilicate precursors (PEG and PVA derived) show resonances at 0 ppm confirming the presence of aluminum nitrate species (ie, Al(VI)), which was added to prepare these precursors. Synthetic aluminosilicate powders demonstrated a peak at 8 ppm indicating the presence of similar aluminum species with minimal environment differences (Figure 3). However, after alkali-activation, all samples exhibit resonances at both ~60 and ~8 ppm, confirming two different atomic environments for the aluminum one for the unreacted aluminum species Al(VI) and the reacted Al(IV) species, composing the aluminosilicate cementitious network.[44,45]

Similarly, $^{1}H$-$^{29}Al$ CP-MAS NMR spectra of all uncalcined synthetic aluminosilicate precursors derived from PEG as well as PVA showed resonance near 0 ppm indicating the presence of Al(VI) species. However, no $^{1}H$-$^{29}Al$ CP MAS NMR signal was observed for all calcined synthetic aluminosilicate powders or geopolymer cements, regardless of polymer cross-linker used (Figure 6). Hence, these results suggest that Al(VI) species were incorporated in the network with oxygen but they were very far from the nearby protons of water or hydroxyls. This observation suggests that water molecules were evaporated due to high temperature of calcination process and polymers were volatilized from the Al–Si network in these calcined precursors, as expected from FTIR results. Similar results for geopolymers indicate the presence of Al(IV) species coordinated with $SiO_4$ in a network with segregated Al(VI) phases as seen in the XRD data (Figure 3) with far protons unsuccessful to transfer nuclei polarization.

## 4 | DISCUSSION

### 4.1 | Effect of polymer architecture (PEG vs PVA)

Differences in polymer architecture, more specifically the absence of hydroxyls (ie, PVA) and presence of ethers (ie, PEG), result in phase segregation within the xerogel and, as a result, form $\gamma$-alumina in the synthetic aluminosilicate powder, as confirmed by XRD (Figure 3) and $^{27}Al$ MAS NMR (Figure 6; Table 4).[46] Moreover, $^{27}Al$ MAS NMR of these PEG-derived aluminosilicate powders (Figure 6) demonstrates that mainly Al(VI) sites exist, as evidenced by the presence of a resonance peak at ~5-9 ppm (Table 4). This finding is seemingly contradictory to the often reported defective spinel structure of $\gamma$-alumina.[47] However, a decrease in the tetragonal nature of $\gamma$-alumina has been observed with increasing temperatures >700°C and adsorption of gases at high temperatures and may be similar to the $\gamma'$-alumina, an anhydrous alumina form as verified by the absence of resonance on $^{27}Al$-$^{1}H$ MAS NMR spectra (Figure 6; Table 4).[35,48] Moreover, contradictory to recent studies,[28,32] the herein study found no evidence of Al(IV) or Al(V) for PVA-L synthetic aluminosilicate powders synthetized at low I/O ratios (ie, high polymer contents). This difference is likely due to the redefinition of the I/O ratio, as explained in Section 2.2.1, and further detailed in the supplementary information.

Limited silicate incorporation into the gel 1 → gel 2 evolution process[49,50] within PEG-derived geopolymer cements may occur as observed by a higher $^{29}Si$ NMR deshielding and higher variability of Si polymerization in FTIR results, when compared to PVA-derived samples as indicated in Tables 2, 3 and 5. The gel 1 has been described as an initial Al-rich binder with a high content of Si–O–Al bonds relative to the bulk Si:Al ratio. This initial gel 1 is said to structurally evolve via condensation of silanols and incorporation of silicon metals, hence increasing the effective Si:Al ratio of the binder.[57] The $^{29}Si$ NMR resonances of PEG-derived geopolymer cements are downfield shifted between −80 and −85 ppm, when compared to PVA-derived geopolymer cements as seen in Table 3. Deshielding of the $^{29}Si$ nuclei may be due to next nearest neighbor (Al) or structural distortions of the gel 2, which are hypothesized to be caused by limited silicate incorporation in the gel 1 precursor.[46] Further confirming these results, FTIR results for PEG-derived geopolymer cements demonstrate geopolymer network formation as observed by peak shifts to lower wave number corresponding to the formation of Si–O–Si and Si–O–Al bonds (1120 $cm^{-1}$ → 1060 $cm^{-1}$), Table 3.[59] Contrastingly, PVA-derived geopolymer cements exhibit greater extent of silicate incorporation in the gel 1 → gel 2 evolution process as sharp and intense absorption peaks are observed to be centered around 1000 $cm^{-1}$.

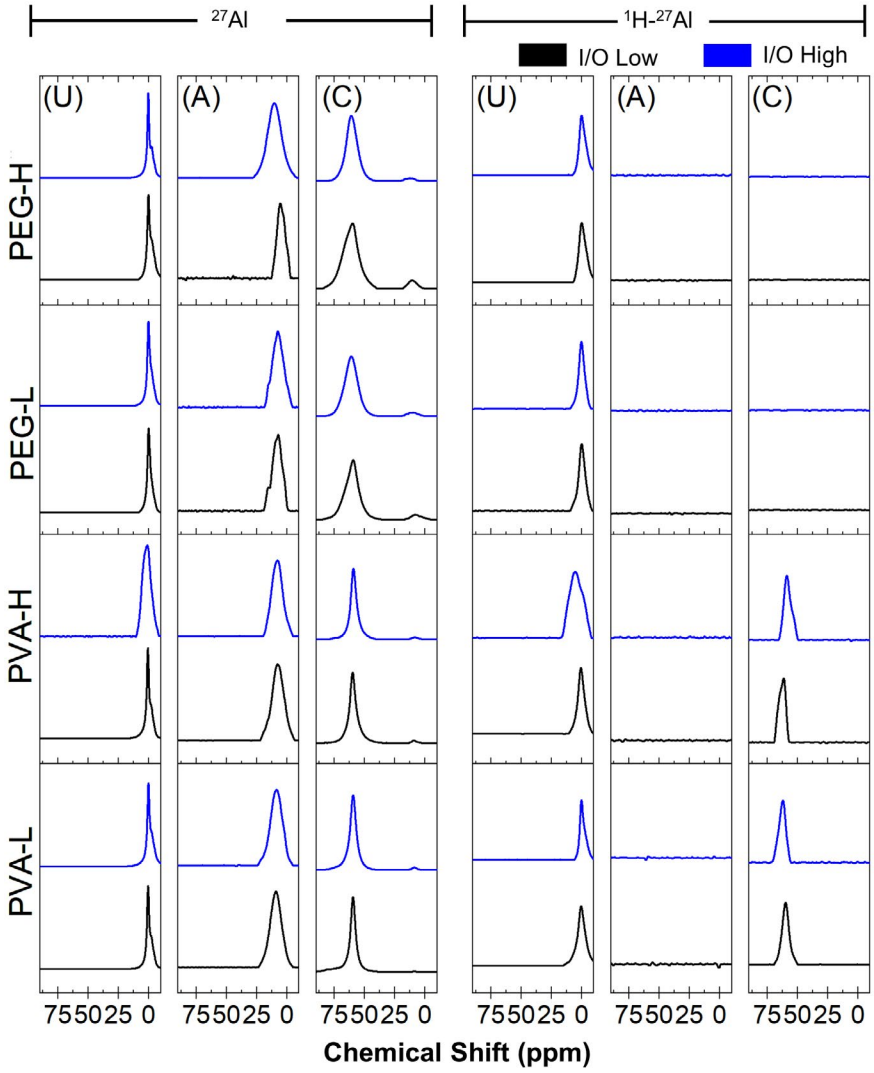


**FIGURE 6** $^{27}$Al MAS NMR and $^{1}$H-$^{27}$Al MAS NMR spectra for uncalcined synthetic aluminosilicate precursors (U), synthetic aluminosilicate powders (A), and geopolymer cements (C) [Color figure can be viewed at wileyonlinelibrary.com]

## 4.2 | Effect of polymer content (I/O ratio: Low vs High)

Decreasing the polymer content (high I/O ratio) reduces Al metal-polymer coordination and results in partial $\gamma$-alumina formation for PEG-derived aluminosilicate powders (see Figure 3). As a result of the decrease polymer-metal coordination, the aluminosilicate powder produced is considered to be of higher reactivity as evidence by the absence of unreacted $Q^4$ as presented in Figure 5. The geopolymer cements resemble PVA-derived geopolymer cements with $Q^4$(4Al) atomic sites. Contrastingly, increasing the polymer content (low I/O) produces geopolymer cements with partial reactivity as evidence by the presence of $Q^4$ and $Q^4$(4Al) silicon sites. At such high polymer contents, incomplete dihydroxylation is also observed in the aluminosilicate powders by the presence of single silanols ($Q^3$) or adjacent water,[55] see Table 5. Similar deshielding has been reported by[43] for Halloysite clays. These results are important as polymer content is evidenced to affect Si–Al atomic coordination. Contrastingly to Refs. [[19,28,32], no presence of Al(IV) or distorted Al(VI) sites has been observed for similar aluminosilicate powders.

## 4.3 | Effect of sol-gel aging conditions (pH: Low vs High)

There are minimal differences in aluminosilicate powders synthetized with low or high pH sol-gel aging conditions indicating that the order of chemical addition bears little effect on the synthesis procedure. For example, PVA-H aluminosilicate powders have slightly higher deshielding of their $^{29}$Si nuclei, as seen in Table 5. Moreover, when compared to samples synthesized with high PVA polymer contents, samples synthesized with a high pH sol-gel aging condition and low PVA polymer contents have a reduction in the absorption peak intensities associated with Si–O–Si and Si–O–Al bonds at ~1060 cm$^{-1}$.[59]

However, when alkali-activated, synthetic aluminosilicate powders produced with low pH sol-gel aging conditions may improve the extent of geopolymerization and dictate the

**TABLE 4** Atomic environment assignments of $^{27}$Al MAS NMR and $^{1}$H-$^{27}$Al MAS NMR spectra for (A) uncalcined precursors, (B) calcined precursors, and (C) geopolymer cements. Assignments are based on Ref. [46]

| | | (A) Uncalcined precursor | | | | (B) Calcined precursor | | | | (C) Geopolymer cement | | | |
|---|---|---|---|---|---|---|---|---|---|---|---|---|---|
| **Sample** | **I/O Ratio** | **$^{27}$Al δ (ppm)** | **Al** | **$^{27}$Al-$^{1}$H δ (ppm)** | **Al** | **$^{27}$Al δ (ppm)** | **Al** | **$^{27}$Al-$^{1}$H δ (ppm)** | **Al** | **$^{27}$Al δ (ppm)** | **Al** | **$^{27}$Al-$^{1}$H δ (ppm)** | **Al** |
| PVA-L | Low | 0.53 | Al(VI) | 0.53 | Al(VI) | 8.53 | Al(VI) | — | — | 59.29 | Al(IV) | 59.68 | Al(IV) |
| | | | | | | | | | | 8.49 | Al(VI) | | |
| | High | 0.13 | Al(VI) | 0.13 | Al(VI) | 8.09 | Al(VI) | — | — | 59.17 | Al(IV) | 61.54 | Al(IV) |
| | | | | | | | | | | 8.5 | Al(VI) | | |
| PVA-H | Low | 0.61 | Al(VI) | 0.61 | Al(VI) | 7.62 | Al(VI) | — | — | 59.67 | Al(IV) | 60.2 | Al(IV) |
| | | | | | | | | | | 9.01 | Al(VI) | | |
| | High | 1.97 | Al(VI) | 1.97 | Al(VI) | 7.39 | Al(VI) | — | — | 59.04 | Al(IV) | 58.97 | Al(IV) |
| | | | | | | | | | | 8.18 | Al(VI) | | |
| PEG-L | Low | 0 | Al(VI) | 0 | Al(VI) | 6.94 | Al(VI) | — | — | 60.16 | Al(IV) | — | — |
| | | | | | | | | | | 7.14 | Al(VI) | | |
| | High | 0.15 | Al(VI) | 0.15 | Al(VI) | 9.26 | Al(VI) | — | — | 60.55 | Al(IV) | — | — |
| | | | | | | | | | | 6.26 | Al(VI) | | |
| PEG-H | Low | 0.1 | Al(VI) | 0.1 | Al(VI) | 5.35 | Al(VI) | — | — | 61.68 | Al(IV) | — | — |
| | | | | | | | | | | 10.48 | Al(VI) | | |
| | High | 0.31 | Al(VI) | 0.31 | Al(VI) | 9.18 | Al(VI) | — | — | 59.88 | Al(IV) | — | — |
| | | | | | | | | | | 6.95 | Al(VI) | | |

**TABLE 5** Atomic environment assignments of $^{29}$Si MAS NMR and $^{1}$H-$^{29}$Si MAS NMR spectra for (a) uncalcined precursors, (b) calcined precursors, and (c) geopolymer cements. Assignments are based on Ref. [40,60]

| | | (a) Uncalcined Precursor | | | | (b) Calcined Precursor | | | | (c) Geopolymer Cement | | | |
|---|---|---|---|---|---|---|---|---|---|---|---|---|---|
| | | $^{29}$Si | | $^{29}$Si-$^{1}$H | | $^{29}$Si | | $^{29}$Si-$^{1}$H | | $^{29}$Si | | $^{29}$Si-$^{1}$H | |
| Sample | I/O Ratio | δ (ppm) | $Q^n$ | δ (ppm) | $Q^n$ | δ (ppm) | $Q^n$ | δ (ppm) | $Q^n$ | δ (ppm) | $Q^n$ | δ (ppm) | $Q^n$ |
| PVA-L | Low | −110.87 | $Q^4$ | −106.8 | $Q^4$ | −111.38 | $Q^4$ | −110.3 | $Q^4$ | −89.95 | $Q^4$ (4Al) | — | — |
| | High | −111.91 | $Q^4$ | — | — | −111.2 | $Q^4$ | −108.02 | $Q^4$ | −88.88 | $Q^4$ (4Al) | −87.5 | $Q^2$ |
| PVA-H | Low | −112.52 | $Q^4$ | −103.6 | $Q^4$ | −109.42 | $Q^4$ | −106.8 | $Q^4$ | −89.34 | $Q^4$ (4Al) | −88.33 | $Q^2$ |
| | High | −110.95 | $Q^4$ | −111 | $Q^4$ | −109.6 | $Q^4$ | −110.37 | $Q^4$ | −87.86 | $Q^4$ (4Al) | −88.14 | $Q^2$ |
| PEG-L | Low | −110.69 | $Q^4$ | −111.8 | $Q^4$ | −109.09 | $Q^4$ | −100 | $Q^3$ | −85.06 | $Q^4$ (4Al) | — | — |
| | | | | | | | | | | −108.55 | $Q^4$ | | |
| | High | −113.16 | $Q^4$ | −102.4 | $Q^3$ | −113.28 | $Q^4$ | −105.8 | $Q^4$ | −80.4 | $Q^4$ (4Al) | −83.52 | $Q^2$ |
| PEG-H | Low | −111.82 | $Q^4$ | −101.8 | $Q^3$ | −109.02 | $Q^4$ | −97 | $Q^3$ | −83.94 | $Q^4$ (4Al) | −84.07 | $Q^2$ |
| | | | | | | | | | | −107.04 | $Q^4$ | | |
| | High | −111.2 | $Q^4$ | −107.4 | $Q^4$ | −112.15 | $Q^4$ | −109.3 | $Q^4$ | −85.26 | $Q^4$ (4Al) | −83.52 | $Q^2$ |

content of silanol groups in the resultant geopolymer cement. PEG-derived geopolymer cements synthesized with low pH sol-gel aging conditions exhibit higher absorption intensities for Si–O–Si and Si–O–Al bonds, when compared to PEG samples produced in high pH conditions (Figure 4). High absorption intensity may indicate a greater extent of silicate incorporation and content of $Q^4$(4Al) units in the geopolymer cements, as previously discussed. Additionally, low pH sol-gel aging conditions yield geopolymer cements with no evidence of geminal silanol groups regardless of polymer used during synthesis.[61] As seen in Figure 5 and indicated in Table 5, no resonance peak is observed for $^{1}$H-$^{29}$Si cross-polarized signal of both PVA-L and PEG-L synthesized with high polymer contents. This result is likely a consequence of the absence of "near protons" and presence of labile water species (indicated by high intensity –OH vibrational stretching, see Figure 4; Tables 2 and 3), which are not near enough for cross-polarization of $^{29}$Si nuclei. Moreover, the absence of silanol groups has been described and explained by Ref. [62] and it is indicative of well-formed geopolymer binders with the majority of framework sites being $Q^4$. Lastly, "traditional" chemical compositions of metakaolin-based geopolymer cements have been reported to exhibit residual silanols from unreacted metakaolin particles, as well as geminal and vicinal silanol groups.[61]

## 4.4 | Natural analog of synthetic aluminosilicates: Metakaolin

All synthesized aluminosilicate precursors approximate the chemical composition of calcined clays (ie, metakaolin) as evidenced by Figure 2.[33] Moreover, similarities to metakaolin are evidenced in both the $^{29}$Si and $^{27}$Al MAS NMR with a resonances near 110 and ~10 ppm corresponding to $Q^4$ Si units and Al(VI), respectively (Tables 4 and 5).[46] In addition, the presence of silanol groups in PEG-derived synthetic aluminosilicate powders at low I/O ratios, is similar to the reported residual silanol groups in metakaolin.[54] Thus, the atomic structure of synthetic aluminosilicate powders may resemble a homogenous mix of $Q^4$ Si units and Al(VI) units with residual silanol groups in particular cases.

However, the structure of synthetic aluminosilicate precursors differs from that of metakaolin due to the absence of $Q^3$ sheet-like Si layers, Al(IV), Al(V), or segregated amorphous alumina phases. In general, metakaolin possesses a broad $^{29}$Si MAS NMR resonance peak at −103 ppm with a linewidth of ~20 ppm, assigned to $Q^3$ "sheet-like" layers,[56] as well as $^{29}$Si resonances corresponding to $Q^4$(1Al) silicon center.[24] Contrastingly, synthesized aluminosilicate powders possess $^{29}$Si MAS NMR resonance peak at −111 ppm, which does not indicate any aluminum bond with silicon. Furthermore, no presence of Al(IV), Al(V), or regions of segregated amorphous alumina are observed in synthesized aluminosilicate powders, as characteristic of the atomic structure of metakaolin.[58]

The presence of extra-framework aluminum (EFAl) was reported in 2012 for metakaolin-based geopolymer cements with Si:Al and Na:Al atomic ratios of 1.6 and 1.0, respectively.[61] The observed structural stability of these cements was attributed to the presence of these tetrahedrally coordinated aluminum ions (ie, Al(IV)). More recently, EFAl with an Al(IV) resonance have been observed in geopolymer cements with Si:Al and Na:Al atomic ratios of 1.50 and 1.18, respectively.[19] Contrastingly, in the present study, $^{27}$Al-$^{1}$H NMR detected the presence of Al(IV) resonances at 60.5 ± 1.5 ppm for PVA-derived geopolymer cements solely, which is in good agreement with results collected from the literature (Table 6). These cross-polarized nuclei resonances have been attributed in other studies to bridging hydroxyl groups (Si–$OH^+$–Al, Brønsted-acid sites).[61] The presence of these hydroxyl groups, both in Si and Al nuclei, have been shown to hydrogen bond with structural

**TABLE 6** NMR peaks detected by various studies on (C)–N-A-S-H cementitious binder variants

| Geopolymer cement | $^{29}$Si NMR (ppm) | $^{27}$Al NMR (ppm) | Reference |
|---|---|---|---|
| $Na_{0.625}Si_{1.00}Al_{0.625}{\cdot}xH_2O$ | −89.0 | 58.0 | [61] |
| $Ca_{0.800}\ Na_{0.078}Si_{1.00}Al_{0.156}{\cdot}xH_2O$ | −75.0, −79.0, −84.0, −86.0, −89.0, −94.0 | 57.0, 0.0 | [15] |
| $Na_{1.00}Si_{1.08}Al_{1.00}{\cdot}xH_2O$ | −86.5, −89.0[a] | 57.4 | [64] |
| $Na_{1.18}Si_{1.5}Al_{1.00}{\cdot}xH_2O$ | — | 61.5, 8.8 | [19] |
| $Na_{\sim 0.015}Si_{1.00}Al_{1.00}{\cdot}xH_2O$ | −87.0, −103.0 | 78.0 | [58] |

[a]The presence of Zeolite A found in samples.

water molecules resulting in the elongation of Al–O bonds.[63] An important observation for the stability and durability of these cements.

Similar to studies of alkali-activated metakaolin, PEG-derived geopolymer cements have resonances at −107 ppm ($Q^4$) from unreacted synthetic aluminosilicate powder (−103 ppm, attributed to $Q^3$ Si-sheets, in metakaolin) and −85 ppm indicative of $Q^4$(4Al) aluminosilicate[56] (Figure 5; Table 6). Similar resonances have been detected in N-A-S-H binder variants, as seen in Table 6. Contrastingly, all PVA-derived geopolymer cements indicate the presence of solely $Q^4$(4Al) aluminosilicate (Figure 5; Table 4), characteristic of N-A-S-H binders of low Si:Al ratios,[58] these also resemble the mineralogy of metakaolin-based cements (Figure 7). In addition, peaks at 800 $cm^{-1}$ are assigned to Al–O stretching in Al(VI) decrease in intensity or are not visible following alkali-activation, suggesting that the octahedral structure breaks down with geopolymerization.[41]

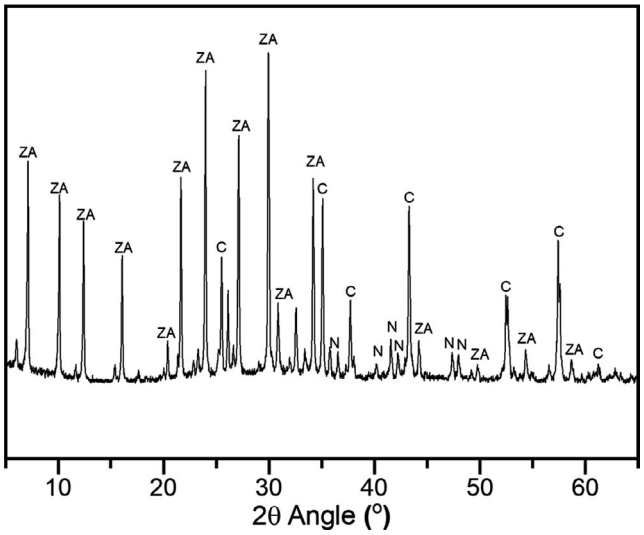


**FIGURE 7** Mineralogy of metakaolin-based samples (Si:Al = 1.0, Na:Al = 1.1) with similar curing conditions confirms similar mineralogy as PVA-derived geopolymer cements. ZA: Zeolite A ($Al_2O_3SiO_2$, PDF# 00-038-0323), N: Sodium Carbonate ($Na_2CO_3$, PDF#01-072-0628), C: Corundum ($Al_2O_3$, internal standard)[38,39]

## 4.5 | Mechanisms of the polymer-assisted sol-gel synthesis

Data collected suggest three possible mechanisms by which the polymer-assisted sol-gel synthesis permits the incorporation of solubilized aluminum ions ($Al^{+3}$). As depicted in Figure 8, $Al^{+3}$ incorporation may be possible by: (a) complexation with polymer cross-linker; (b) hydrogen bonding with silanol; and (c) competition between these two complexation mechanisms. These will be discussed in the following sections.

### 4.5.1 | Polymer cross-linker complexation of $Al^{+3}$ metal ions

Architecture differences in polymer cross-linker oxide (ie, ether, hydroxyl) may influence the polymer-metal interactions of $Al^{+3}$ ions by inducing metal complexation or hydrogen bonding. Given that oxygen is a strong electron donor in both PVA and PEG systems, the electron-poor aluminum metal would tend to associate with these atoms to form complexes.[65] Evidence for such metal-polymer complexes is observed for PVA-derived uncalcined synthetic aluminosilicate precursors indicated by a shift of a vibrational peak centered around 1750 $cm^{-1}$ in reagent PVA to 1730 $cm^{-1}$ after polymer-assisted sol-gel synthesis. The shift of this peak may indicate polymer-metal interactions between residual carbonyl groups on PVA polymer cross-linkers (an artifact from commercial fabrication of PVA from poly(vinyl acetate)) and the aluminum metal (at 1730 $cm^{-1}$) (Figure 4).[66] Changes in vibrational energy toward lower wavenumbers following interactions with metals have previously been attributed to metal-ion complexation with the carbonyl (C–O) moiety in PVA.[66,67]

For PEG-derived uncalcined synthetic aluminosilicate precursors, previous literature suggests that $Al^{+3}$ polymer coordination occurs in the C–O–C stretching region between 1110 and 1105 $cm^{-1}$.[68] For this system, the 1100 $cm^{-1}$ region corresponds to Si–O–Si vibrational stretching and bending frequencies, thus hindering the analysis of metal-polymer coordination for PEG-based systems. For both polymeric systems, it can be speculated that the hydration of components by

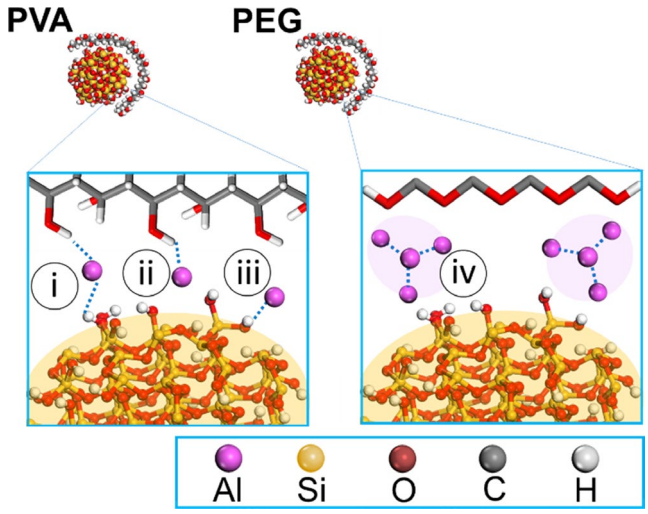


**FIGURE 8** Hypothesized mechanisms of polymer-assisted sol-gel synthesis: (i) ionic competition between polymer cross-linker coordination and silanol-based polycondensation; (ii) complexation with polymer cross-linker; (iii) hydrogen bonding with silanol group; and (iv) poor homogenization and phase segregation, as observed for PEG-derived calcined precursors [Color figure can be viewed at wileyonlinelibrary.com]

water during the sol-gel aging would enable hydrogen bonding between water and pendant hydroxyl units, and as the xerogels develop (ie, dehydration), metal coordination may be enhanced as with less volume the materials are more likely to interact. For both PEG and PVA systems, following calcination, the vibrational bands at 1730 $cm^{-1}$ as well as broad vibrational bands from 3500 to 3000 $cm^{-1}$ corresponding to O–H stretching frequency in both PVA- and PEG-derived synthetic aluminosilicate powders decrease in intensity. This decrease in intensity may indicate that the polymer, nitrate counterion, and water were effectively removed following calcination, likely disrupting the $Al^{+3}$ polymer coordination. Such disruptions may explain the absence of Al(IV) and distorted Al(VI) sites in the aluminosilicate powder, contrary to published literature.[19,28,32]

### 4.5.2 | Silanol coordination of $Al^{+3}$ metal ions

$^{29}$Si MAS NMR (Figure 5; Table 5) does not reveal bulk aluminum incorporation in the xerogels of the uncalcined synthetic aluminosilicate precursor; however; cross-polarization data on these gels suggest the possibility of coordination and sparse hydrogen bonding between silanol and aluminum ions in certain synthesis conditions. However, determination of different $Q^4$(nAl) sites may be determined based on peak maxima with linewidths of 10 ppm, as described in Ref. [33,69], $^{29}$Si MAS NMR spectra collected herein demonstrates the single-phase purity of precursors, due to narrower linewidths than reported in literature and high upfield resonances. As seen in Table 5, uncalcined synthetic aluminosilicate precursors demonstrate peak resonances at −111 ppm that are attributed to $Q^4$ silicon sites. Furthermore, narrow line widths between 8.3 and 17.4 ppm (Figure 5) render the determination of different $Q^4$(nAl) sites inappropriate, as aforementioned, and no FTIR evidence specifically supports the presence of corresponding Si–O–Al bonds in uncalcined synthetic aluminosilicate precursors, even though vibrational frequency corresponding to Si–O–Si asymmetric stretching is observed (Figure 4; Tables 2 and 3). However, $^{29}$Si CP MAS-NMR signal provides spectra of nuclei spatially close to immobilized hydroxyls, structural water molecules, or other protonated species, typically less than 5 Å.[69] As observed in Table 3, all uncalcined synthetic aluminosilicate precursors exhibit cross polarization resonances which provide further evidence of $Q^4$ silicon atomic sites interacting with hydrous species, possibly from the water shell associated with $Al^{+3}$ cations (ie, Al(VI)). In addition, the presence of single silanol groups ($Q^3$, −100 ppm) remaining in PEG-derived samples aged at high pH values and low I/O suggest the possibility for hydrogen bonding between silica particles and $Al^{+3}$ cations.

FTIR can be used to suggest mechanisms of inter- and intra-molecular coordination, such as hydrogen bonding in the xerogel. For both polymer architectures in the xerogel, the vibrational peak at 1650 $cm^{-1}$ is attributed to H–O–H bending vibrations[70] and is present in the FTIR of silica, aluminum nitrate, and PVA starting materials but at a lesser intensity than in the xerogel. The peak centered at 1650 $cm^{-1}$ in conjunction with the broad stretching vibration of –OH centered at approximately 3400 $cm^{-1}$ are often attributed to hydrogen bonding or water adsorption.[71–74] For all xerogel materials, there is an increase in the intensity of these two vibrational frequencies. The increase in intensity may be attributed to hydrogen bonding between hydroxyl units between the polymers, silica, and bound water or to coordination of the silanol to aluminum following xerogel formation (Figure 8I).[71,75] The changes in these molecular vibrations do not specifically indicate that silanol is coordinating with aluminum oxide but can suggest this mechanism along with other hydrogen bonding mechanisms.

## 5 | FUTURE WORK

In this work, it has been shown that control of the I/O ratio (ie, polymer content) in polymer-assisted sol-gel synthesis methods is imperative to produce adequate aluminosilicate powders for alkali-activation. Contrary to previous publications by Ref. [19,28,32], the presence of Al(IV) or distorted Al(VI) was not observed likely due to differences in the polymer content (ie, I/O ratio). As explained in Section 4.5.1,

based on previous literature it is known that $Al^{+3}$ metal-polymer coordination occurs in the C–O–C stretching region between 1110 and 1105 $cm^{-1}$.[71] Consequently, polymer cross-linker complexation of $Al^{+3}$ metal ions is expected to be the dominant mechanism for producing high-reactivity aluminosilicate powders, hence, explaining the differences in results observed in this study. Thus, further research to probe the mechanisms of polymer-assisted sol-gel is crucial for the replicability and optimization of this synthesis technique.

Mechanisms of polymer-assisted sol-gel are important to leverage the creation of N-A-S-H cements with different atomic structures. Molecular dynamic simulations or further atomic statistical thermodynamic computational modeling is necessary to understand the kinetics and energetic favorability of these synthesis mechanisms. Once these mechanisms are further understood, their application to low-calcium AACs and geopolymer systems may yield important insights into the formation of differing hydroxyl groups, observed herein. In addition, different synthesis pathways for geopolymer cements result in different silanol contents. These results must be verified via a carefully optimized contact time to examine cross-polarization efficiency. An important gap in knowledge is the effect of hydroxyl groups on macro properties of low-calcium cementitious binders. For example, the role of hydroxyl groups on drying shrinkage properties or water transport has not yet been investigated. Lastly, further exploration of polymer-assisted sol-gel synthesis will enable the study of novel single-phase binders—an important scientific pursuit that is currently in progress by the authors.

## 6 | CONCLUSION

This study investigated the effects of polymer architecture (ie, PVA vs PEG), polymer content (ie, low vs high ion-to-polymer-oxide (I/O) atomic ratio), and sol-gel aging pH conditions (ie, low vs high) on the atomic structure of resultant synthetic aluminosilicate powders and geopolymer cements. The results have shown that the polymer architecture is a primary factor in controlling phase segregation in synthetic aluminosilicate powders and the resulting mineralogy of geopolymer cements. The use of FTIR, XRD, and $^{29}Si$ and $^{27}Al$ single pulse and $^{1}H$ cross-polarized MAS NMR confirmed the effect of polymer architecture on the metal complexation of $Al^{+3}$ ions, while PEG polymers yielded phase segregation during synthesis and formation of $\gamma$-alumina with a predominance of Al(VI) sites. Contrastingly, it is observed that the presence of hydroxyls in PVA may provide higher ion coordination competition, which results in synthetic aluminosilicate powders and geopolymer cements with single atomic environments. Moreover, PEG-derived synthetic aluminosilicate powders are most similar to the atomic environment of metakaolin (ie, calcined clay).

A decrease in polymer content during synthesis is observed to improve reactivity of the precursor improving the extent of binder formation in these samples. While sol-gel pH aging conditions (affected by order of reactant addition) reveals the ability to influence the content of Brønsted-acid sites (–OH groups) near the aluminum nuclei and germinal silanol groups within geopolymer cements. As a result, the molecular structure and mineralogy of resultant geopolymer cements are affected in the following order of significance: polymer type > polymer content > sol-gel pH aging condition. Finally, metakaolin-based geopolymers resemble the molecular structure and mineralogy of PVA-derived geopolymer cements. Thus, validating the further use of metakaolin as an aluminosilicate precursor to produce highly pure N-A-S-H cementitious binders.

Evidence collected supports three possible mechanisms by which the polymer-assisted sol-gel synthesis permits the incorporation of solubilized aluminum ions ($Al^{+3}$) and formation of N-A-S-H (sodium-aluminum-silicate-hydrate) geopolymer binders. The proposed mechanisms are hypothesized to be related to: (a) complexation with polymer cross-linker; (b) hydrogen bonding with silanol; and (c) competition between polymer cross-linker coordination and silanol-based polycondensation. It is expected that $Al^{+3}$ metal-polymer competition dominates the mechanism for the production of high-reactivity aluminosilicate powders. However, further understanding on these synthesis mechanisms is imperative to permit the design and synthesis of tailored nanostructures of low-calcium AACs and geopolymer cements.

## ACKNOWLEDGMENTS

This research was made possible by the Department of Civil, Environmental, and Architectural Engineering, the College of Engineering and Applied Sciences, and the Sustainable Infrastructure Materials Laboratory (SIMLab) at the University of Colorado Boulder. This work was supported by the National Science Foundation grants CBET-1604457 and CMMI-1727788. Dr Kate Campbell and Mr Tyler Kane of the United States Geological Survey (USGS) are gratefully acknowledged for their assistance with XRD. Dr Amanda Garley is gratefully acknowledged for her assistance in visualization of this work. This work represents the views of the authors and not necessarily those of the sponsors.

## ORCID

*Juan Pablo Gevaudan* https://orcid.org/0000-0001-6843-9747

*Wil V. Srubar* https://orcid.org/0000-0001-8226-2458

## REFERENCES


1. Wright JD, Sommerdijk N. Sol-gel materials: chemistry and applications. Boca Raton, FL: CRC Press, 2014;p. 1–125.
2. King G. Methods for hydrolysis of alkoxysilanes for use in paints, dental cements, treatment of brick, stone and concrete. Paint Test Man. 1931;1(16–20):52–5.
3. Pierre AC. Introduction to sol-gel processing, vol. 1. Berlin: Springer Science & Business Media; 2013.
4. Danks AE, Hall SR, Schnepp Z. The evolution of "sol-gel" chemistry as a technique for materials synthesis. Mater Horiz. 2016;3:91–112.
5. Xi LI, Baokun XU, Zichen W, Feng C, Muyu Z. Preparation of nanocrystalline materials of perovskite-type $La_{1-x}Sr_xFeO_3$ (x= 0, 0.1, 0.2, and 0.4) by using gel of poly(ethylene glycol). J Mater Sci Lett. 1992;11:1476–8.
6. Li X, Zhang H, Chi F, Li S, Xu B, Zhao M. Synthesis of nanocrystalline composite oxides $La_{1-x}Sr_xFe_{1-y}Co_yO_3$ with the perovskite structure using polyethylene glycol-gel method. Mater Sci Eng B. 1993;18:209–13.
7. Pramanik P, Pathak A. A new chemical route for the preparation of fine ferrite powders. Bull Mater Sci. 1994;17(6):967–75.
8. Kumar Saha S, Pathak A, Pramanik P. Low-temperature preparation of fine particles of mixed oxide systems. J Mater Sci Lett. 1995;14(1):35–7.
9. Li X, Zhang H, Zhao M. Preparation of nanocrystalline $LaFeO_3$ using reverse drop coprecipitation with polyvinyl alcohol as protecting agent. Mater Chem Phys. 1994;37(2):132–5.
10. Sun Y-K, Oh I-H. Preparation of ultrafine $YBa_2Cu_3O_{7-x}$ superconductor powders by the Poly(vinyl alcohol)-assisted sol-gel method. Ind Eng Chem Res. 1996;35:4296–300.
11. Gulgun MA, Nguyen MH, Kriven WM. Polymerized organic—inorganic synthesis of mixed oxides. J Am Ceram Soc. 1999;82(3):556–60.
12. Kriven WM, Lee SJ, Gulgun M. Synthesis of oxide powders via polymeric steric entrapment. Ceram Trans. 1999;108:99–110.
13. Walkley B, Provis JL, San Nicolas R, Sani M-A, van Deventer J. Stoichiometrically controlled C–(A)–S–H/N-A-S-H gel blends via alkali-activation of synthetic precursors. Adv Appl Ceram. 2015;114(7):372–7.
14. Walkley B, San Nicolas R, Sani M-A, Bernal SA, van Deventer J, Provis JL. Structural evolution of synthetic alkali-activated CaO-MgO-$Na_2O$-$Al_2O_3$-$SiO_2$ materials is influenced by Mg content. Cem Concr Res. 2017;99(May):155–71.
15. Walkley B, San Nicolas R, Sani M-A, Rees GJ, Hanna JV, van Deventer J, et al. Phase evolution of C-(N)-A-S-H/N-A-S-H gel blends investigated via alkali-activation of synthetic calcium aluminosilicate precursors. Cem Concr Res. 2016;1(89):120–35.
16. Lee SJ, Kriven WM. Synthesis and hydration study of Portland cement components prepared by the organic steric entrapment method. Mater Struct Constr. 2005;38(275):87–92.
17. Walkley B, San Nicolas R, Bernal S. Effect of MgO incorporation on the structure of synthetic alkali-activated calcium aluminosilicate binders. Conf 27th Bienn Natl Conf Concr Inst Aust; August; 2015.
18. Walkley B, San Nicolas R, Sani M-A, Gehman JD, van Deventer J, Provis JL. Synthesis of stoichiometrically controlled reactive aluminosilicate and calcium-aluminosilicate powders. Powder Technol. 2016;1(297):17–33.
19. Walkley B, Rees GJ, San Nicolas R, Van Deventer J, Hanna JV, Provis JL. New structural model of hydrous sodium aluminosilicate gels and the role of charge-balancing extra-framework Al. J Phys Chem C. 2018;122(10):5673–85.
20. Vafaei M, Allahverdi A, Dong P, Bassim N. Acid attack on geopolymer cement mortar based on waste-glass powder and calcium aluminate cement at mild concentration. Constr Build Mater. 2018;30(193):363–72.
21. Palomo A, Blanco-Varela M, Granizo M, Puertas F, Vazquez T, Grutzeck M. Chemical stability of cementitious materials based on metakaolin. Cem Concr Res. 1999;29(7):997–1004.
22. Fernandez-Jimenez A, García-Lodeiro I, Palomo A. Durability of alkali-activated fly ash cementitious materials. J Mater Sci. 2007;42:3055–65.
23. Kriven WM, Bell JL, Gordon M. Microstructure and microchemistry of fully-reacted geopolymers and geopolymer matrix composites. Ceram Trans. 2015;153:227–50.
24. Duxson P, Provis JL, Lukey GC, Separovic F, Van DJ. $^{29}Si$ NMR study of structural ordering in aluminosilicate geopolymer gels. Langmuir. 2005;21:3028–36.
25. Duxson P, Fernández-Jiménez A, Provis JL, Lukey GC, Palomo A, van Deventer J. Geopolymer technology: the current state of the art. J Mater Sci. 2007;42(9):2917–33.
26. Palomo A, Fernández-Jiménez A, Criado M. "Geopolymers": same basic chemistry, different microstructures. Mater Construccion. 2004;54(275):77–91.
27. Singh JP, Bansal NP, Kriven WM. American Ceramic Society. Advances in ceramic matrix composites X: proceedings of the 106th Annual Meeting of the American Ceramic Society: Indianapolis, Indiana, USA (2004). Wiley InterScience (Online service). American Ceramic Society; 2005. 182 p.
28. Walkley B, San Nicolas R, Sani MA, Gehman JD, Van Deventer J, Provis JL. Phase evolution of $Na_2O$-$Al_2O_3$-$SiO_2$-$H_2O$ gels in synthetic aluminosilicate binders. Dalton Trans. 2016;45(13): 5521–35.
29. Craun Z. The role of magnesium in the acid degradation of metakaolin-based alkali-activated cements. Civil Engineering Graduate Theses & Dissertations [Internet]. Jan 1 2018; Available from: https://scholar.colorado.edu/cven_gradetds/352.
30. Farrell RF, Matthes SA, Mackie AJ. A simple, low-cost method for the dissolution of metal mineral samples in plastic pressure vessels. US Bureau Mines Rep. 1980;(BM-RI-8480):19.
31. User E. Guide to RockJock—a program for determining quantitative mineralogy from X-ray diffraction data. US Geol Surv Open-File Rep. 2003;47. 1–47.
32. Walkley B, San Nicolas R, Sani MA, Gehman JD, van Deventer J, Provis JL. Synthesis of stoichiometrically controlled reactive aluminosilicate and calcium-aluminosilicate powders. Powder Technol. 2016;297:17–33.
33. Gevaudan JP, Campbell KM, Kane TJ, Shoemaker RK, Srubar WV. Mineralization dynamics of metakaolin-based alkali-activated cements. Cem Concr Res. 2017;94:1–12.
34. Shirai T, Watanabe H, Fuji M, Takahashi M. Structural properties and surface characteristics on aluminum oxide powders. Annu Rep Adv Ceram Res Cent Nagoya Inst Technol. 2009;9:23–31.
35. Paglia G, Buckley CE, Rohl AL, Hart RD, Winter K, Studer AJ, et al. Boehmite derived γ-alumina system. 1. Structural evolution with temperature, with the identification and structural determination of a new transition phase, γ′-alumina. Chem Mater. 2004;16(2):220–36.
36. Tilley DB, Eggleton RA. The natural occurrence of eta-alumina (n-$Al_2O_3$) in bauxite. Clays Clay Mater. 1996;44(5):658–64.

37. Alex TC, Sasi Kumar C, Kailath AJ, Kumar R, Roy SK, Mehrotra SP. Analysis of mechanically induced reactivity of boehmite using kinetics of boehmite to $\gamma$-$Al_2O_3$ transformation. Metall Mater Trans B Process Metall Mater Process Sci. 2011;42(3):592–603.
38. Flanigen E, Grose R. Phosphorous substitution in zeolite frameworks. Adv Chem. 1971;101:76–101.
39. Shirasuka K, Yanagida H, Yamaguchi G. The preparation of eta alumina and its structure. Yogyo Kyokai Shi. 1976;84:610–3.
40. Rios CA, Williams CD, Fullen MA. Nucleation and growth history of zeolite LTA synthesized from kaolinite by two different methods. Appl Clay Sci. 2009;42(3–4):446–54.
41. Zhang Z, Wang H, Provis JL, Bullen F, Reid A, Zhu Y. Quantitative kinetic and structural analysis of geopolymers. Part 1. the activation of metakaolin with sodium hydroxide. Thermochim Acta. 2012;539:23–33.
42. Myronyuk IF, Mandzyuk VI, Sachko VM, Gun'ko VM. Structural and morphological features of disperse alumina synthesized using aluminum nitrate nonahydrate. Nanoscale Res Lett. 2016;11(1):153.
43. Thompson JG. Interpretation of solid $^{13}C$ and $^{29}Si$ nuclear magnetic resonance spectra of kaolinite intercalates. Clays Clay Mater. 1985;33(3):173–80.
44. Stebbins JF, Lee SK, Oglesby JV. Al-O-Al oxygen sites in crystalline aluminates and aluminosilicate glasses: high-resolution oxygen-$^{17}$NMR results. Am Miner. 1999;84(5-6):983–6.
45. Skibsted J, Henderson E, Jakobsen HJ. Characterization of calcium aluminate phases in cements by aluminum-27 MAS NMR spectroscopy. Inorg Chem. 1993;32(6):1013–27.
46. Smith ME, Mackenzie K. Multinuclear solid state NMR of inorganic materials. Pergamon Mater Ser; 2002;6:201–242.
47. Lee M-H, Cheng C-F, Heine V, Klinowski J. Distribution of tetrahedral and octahedral A1 sites in gamma alumina. Chem Phys Lett. 1997;265(6):673–6.
48. Rohner M, Sharma VK, Richarz W. A magic angle spinning $^{27}Al$ NMR study of the adsorption of CL2 on $\gamma$-alumina. Can J Chem Eng. 1989;67(3):513–5.
49. White CE, Provis JL, Llobet A, Proffen T, van Deventer J. Evolution of local structure in geopolymer gels: an *in situ* neutron pair distribution function analysis. J Am Ceram Soc. 2011;94(10):3532–9.
50. Fernández-Jiménez A, Palomo A, Sobrados I, Sanz J. The role played by the reactive alumina content in the alkaline activation of fly ashes. Microporous Mesoporous Mater. 2006;91(1):111–9.
51. Granizo ML, Alonso S, Blanco-Varela MT, Palomo A. Alkaline activation of metakaolin: effect of calcium hydroxide in the products of reaction. J Am Ceram Soc. 2002;85(1):225–31.
52. Zhang Y, Sun W, Li Z. Infrared spectroscopy study of structural nature of geopolymeric products. J Wuhan Univ Technol-Mater Sci Ed. 2008;23(4):522–7.
53. Alkan M, Hopa Ç, Yilmaz Z, Güler H. The effect of alkali concentration and solid/liquid ratio on the hydrothermal synthesis of zeolite NaA from natural kaolinite. Microporous Mesoporous Mater. 2005;86(1–3):176–84.
54. Rocha J, Klinowski J. Solid-state NMR studies of the structure and reactivity of metakaolinite. Angew Chem Int Ed Engl. 1990;29(5):553–4.
55. Maciel GE, Sindorf DW. Silicon-29 nuclear magnetic resonance study of the surface of silica gel by cross polarization and magic-angle spinning. J Am Chem Soc. 1980;102(25):7606–7.
56. Singh PS, Trigg M, Burgar I, Bastow T. Geopolymer formation processes at room temperature studied by $^{29}Si$ and $^{27}Al$ MAS-NMR. Mater Sci Eng A. 2005;396(1–2):392–402.
57. Provis JL, Palomo A, Shi C. Advances in understanding alkali-activated materials. Cem Concr Res. 2015;78:110–25.
58. Weng L, Sagoe-Crentsil K. Dissolution processes, hydrolysis and condensation reactions during geopolymer synthesis: part I—low Si/Al ratio systems. J Mater Sci. 2007;42(9):2997–3006.
59. Vidal L, Joussein E, Colas M, Cornette J, Sanz J, Sobrados I, et al. Controlling the reactivity of silicate solutions: a FTIR, Raman and NMR study. Colloids Surf Physicochem Eng Asp. 2016;503:101–9.
60. Klinowski J. Nuclear magnetic resonance studies of zeolites. Prog NMR Spectrosc. 1984;16(C):237–309.
61. Brus J, Kobera L, Urbanová M, Koloušek D, Kotek J. Insights into the structural transformations of aluminosilicate inorganic polymers: a comprehensive solid-state NMR study. J Phys Chem C. 2012;116(27):14627–37.
62. Provis JL, Harrex RM, Bernal SA, Duxson P, van Deventer J. Dilatometry of geopolymers as a means of selecting desirable fly ash sources. J Non-Cryst Solids. 2012;358(16):1930–7.
63. Hou D, Zhang YU, Yang T, Zhang J, Pei H, Zhang J, et al. Molecular structure, dynamics, and mechanical behavior of sodium aluminosilicate hydrate (NASH) gel at elevated temperature: A molecular dynamics study. Phys Chem Chem Phys. 2018;20(31):20695–711.
64. Rowles MR, Hanna JV, Pike KJ, Smith ME, O'Connor BH. $^{29}Si$, $^{27}Al$, $^{1}H$ and $^{23}Na$ MAS NMR study of the bonding character in aluminosilicate inorganic polymers. Appl Magn Reson. 2007;32(4):663–89.
65. Chen H, Jiang C, Wu H, Chang F. Hydrogen bonding effect on the poly (ethylene oxide), phenolic resin, and lithium perchlorate–based solid-state electrolyte. J Appl Polym Sci. 2004;91(2):1207–16.
66. Füllbrandt M, Purohit PJ, Schönhals A. Combined FTIR and dielectric investigation of poly (vinyl acetate) adsorbed on silica particles. Macromolecules. 2013;46(11):4626–32.
67. Gan Y, Bai S, Hu S, Zhao X, Li Y. Reaction mechanism of thermally-induced electric conduction of poly (vinyl alcohol)–silver nitrate hybrid films. RSC Adv. 2016;6(61):56728–37.
68. Wieczorek W, Raducha D, Zalewska A, Stevens JR. Effect of salt concentration on the conductivity of PEO-based composite polymeric electrolytes. J Phys Chem B. 1998;102(44):8725–31.
69. Brus J, Abbrent S, Kobera L, Urbanova M, Cuba P. Advances in 27 Al MAS NMR studies of geopolymers. Annu Rep Nmr Spectro. 2016; 88: 79–147.
70. Ramasesha K, De Marco L, Mandal A, Tokmakoff A. Water vibrations have strongly mixed intra- and intermolecular character. Nat Chem. 2013;22(5):935.
71. Asay DB, Kim SH. Evolution of the adsorbed water layer structure on silicon oxide at room temperature. J Phys Chem B. 2005;109(35):16760–3.
72. Reis E, Campos FS, Lage AP, Leite RC, Heneine LG, Vasconcelos WL, et al. Synthesis and characterization of poly (vinyl alcohol) hydrogels and hybrids for rMPB70 protein adsorption. Mater Res. 2006;9(2):185–91.
73. Sudhamani SR, Prasad MS, Sankar KU. DSC and FTIR studies on gellan and polyvinyl alcohol (PVA) blend films. Food Hydrocoll. 2003;17(3):245–50.
74. Chen T, Wu Z, Wei W, Xie Y, Wang X, Niu M, et al. Hybrid composites of polyvinyl alcohol (PVA)/Si–Al for improving the

properties of ultra-low density fiberboard (ULDF). RSC Adv. 2016;6(25):20706–12.

75. Luo Y, Jiang X, Zhang W, Li X. Effect of aluminium nitrate hydrate on the crystalline, thermal and mechanical properties of poly (vinyl alcohol) film. Polym Polym Compos. 2015;23(8):555.

## SUPPORTING INFORMATION

Additional supporting information may be found online in the Supporting Information section at the end of the article.

**How to cite this article:** Gevaudan JP, Wallat JD, Lama B, Srubar WV III. PVA- and PEG-assisted sol-gel synthesis of aluminosilicate precursors for N-A-S-H geopolymer cements. *J Am Ceram Soc*. 2020;103:859–877. https://doi.org/10.1111/jace.16764